D atom loss in the photodissociation of the DNCN radical: Implications for prompt NO formation

David E. Szpunar,[a] Ann Elise Faulhaber, Kathryn E. Kautzman, Paul E. Crider II, and Daniel M. Neumark[b]
Department of Chemistry, University of California, Berkeley, California 94720
and Chemical Sciences Division, Lawrence Berkeley National Laboratory, Berkeley, California 94720

(Received 21 November 2006; accepted 25 January 2007; published online 21 March 2007)

The photodissociation of DNCN following excitation of the $\tilde{C}\,^2A'' \leftarrow \tilde{X}\,^2A''$ electronic transition was studied using fast beam photofragment translational spectroscopy. Analysis of the time-of-flight distributions reveals a photodissociation channel leading to D+NCN competitive with the previously observed $CD+N_2$ product channel. The translational energy distributions describing the D+NCN channel are peaked at low energy, consistent with internal conversion to the ground state followed by statistical decay and the absence of an exit barrier. The results suggest a relatively facile pathway for the reaction $CH+N_2 \rightarrow H+NCN$ that proceeds through the HNCN intermediate and support a recently proposed mechanism for prompt NO production in flames. © *2007 American Institute of Physics*. [DOI: 10.1063/1.2710271]

I. INTRODUCTION

The HNCN radical has attracted interest as a possible intermediate in prompt NO formation initiated by the reaction of CH with N_2.[1,2] Prompt NO is thus called because it is formed in the primary reaction zone of a hydrocarbon flame, where temperatures are too low for the well-understood thermal NO mechanism (initiated by $O+N_2 \rightarrow NO+N$) to operate. The observation of NO in this region requires a lower-energy mechanism for splitting the N_2 bond.[3,4] The reaction of CH with N_2 has long been studied as the most likely initial step in prompt NO formation.[1,3,5–18] One possible route for this reaction proceeds through rearrangement of the CHN_2 complex to form the HNCN intermediate, followed by dissociation. Therefore, studying the photodissociation dynamics of the HNCN radical enables one to probe directly the $CH+N_2$ reaction through the HNCN intermediate by examining the corresponding half reaction, HNCN → products, under well-controlled conditions. In this work, we build on our previous studies of the photodissociation of the HNCN and DNCN radicals[2] and the related HCNN radical[19] by investigating the D atom loss channel of DNCN.

While much attention was initially focused on the reaction $CH(\tilde{X}\,^2\Pi)+N_2 \rightarrow HCN+N(^4S)$ as a possible first step in this mechanism due to its plausible thermodynamics (it is endothermic by only about 0.1 eV),[7] the reaction is spin forbidden, casting some doubt on whether it could proceed fast enough to explain observed NO formation rates. These reservations were quantified by Cui *et al.*,[17] who calculated the predicted thermal rate constant to be two orders of magnitude too low to account for the experimental results.

An alternative first step for prompt NO formation, the reaction $CH(\tilde{X}\,^2\Pi)+N_2 \rightarrow H+NCN$, was proposed by Moskaleva *et al.*[1] The proposed pathway for this reaction involved the formation of a cyclic C_{2v} intermediate, followed by isomerization to a much more stable intermediate, HNCN, which then dissociates to H+NCN (see Fig. 1). While the $H(^2S)+NCN(\tilde{X}\,^3\Sigma_g^-)$ products are less thermodynamically favorable than $N(^4S)+HCN$ (the reaction is endothermic by about 0.9 eV), the H+NCN products are spin allowed, lie slightly lower in energy than the final transition state along the pathway to $N(^4S)+HCN$, and should be reached without an exit barrier. Support for this mechanism has come from the recent laser-induced fluorescence detection of NCN in flames.[20] This evidence for HNCN as an important combustion intermediate has provided motivation for its further study.

HNCN and DNCN have been the subject of several spectroscopic[2,21–27] and theoretical[1,23,28–30] investigations. The HNCN $\tilde{B}\,^2A' \leftarrow \tilde{X}\,^2A''$ transition, with its origin at 28 994 cm^{-1}, has been observed in several laboratories.[2,21,25] A progression of higher-energy features, beginning at

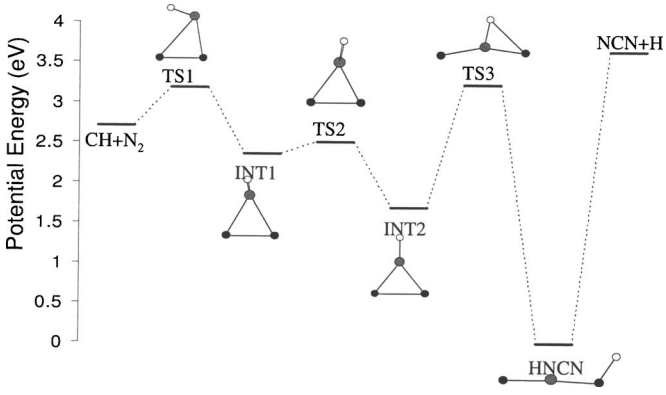

FIG. 1. Stationary points along the $CH+N_2 \rightarrow H+NCN$ reaction pathway, based on the energies determined by Moskaleva *et al.* (Ref. 1).

[a]Present address: Department of Biological, Chemical and Physical Sciences, Roosevelt University, Chicago, IL 60605.
[b]Author to whom correspondence should be addressed. Electronic mail: dneumark@berkeley.edu

30 475 cm^{-1} has also been studied.[24,26,27] Photofragment yield spectra[2] revealed that all but the lowest-energy member of this progression lead to photofragments via predissociation, and the features were assigned to a NCN symmetric stretch progression in the $\tilde{C}\,^2A'' \leftarrow \tilde{X}\,^2A''$ electronic transition.

Our previous study of the photodissociation of HNCN and DNCN focused on the dissociation dynamics following excitation to the $\tilde{B}\,^2A'$ and $\tilde{C}\,^2A''$ states. At those excitation energies, the product channels shown below, along with their heats of reaction $\Delta_{rxn}H_0$, were energetically allowed[2] [channel (5) is allowed only when the $\tilde{C}\,^2A'' \leftarrow \tilde{X}\,^2A''$ transition is excited]:

$$\mathrm{HNCN}(\tilde{X}\,^2A'') + h\nu$$

$$\rightarrow \mathrm{N_2}(\tilde{X}\,^1\Sigma_g^+) + \mathrm{CH}(\tilde{X}\,^2\Pi), \quad 2.80 \pm 0.03\ \mathrm{eV}, \tag{1}$$

$$\rightarrow \mathrm{HCN}(\tilde{X}\,^1\Sigma^+) + \mathrm{N}(^4S), \quad 2.87 \pm 0.05\ \mathrm{eV}, \tag{2}$$

$$\rightarrow \mathrm{HNC}(\tilde{X}\,^1\Sigma^+) + \mathrm{N}(^4S), \quad 3.45 \pm 0.05\ \mathrm{eV}, \tag{3}$$

$$\rightarrow \mathrm{N_2}(\tilde{X}\,^1\Sigma_g^+) + \mathrm{CH}(\tilde{a}\,^4\Sigma), \quad 3.54 \pm 0.03\ \mathrm{eV}, \tag{4}$$

$$\rightarrow \mathrm{H}(^2S) + \mathrm{NCN}(\tilde{X}\,^3\Sigma_g^-), \quad 3.72 \pm 0.04\ \mathrm{eV}. \tag{5}$$

The only product channel observed was $\mathrm{N_2}(\tilde{X}\,^1\Sigma_g^+) + \mathrm{CH}(\tilde{X}\,^2\Pi)$, channel (1), and the translational energy distributions suggested internal conversion to the ground state followed by dissociation through a cyclic transition state, consistent with the reaction pathway proposed by Moskaleva *et al.*[1] However, the coincidence detection setup used in our earlier study was not suited for the detection of fragment pairs with mass ratios higher than about 4:1, so that products from channel (5) could not have been detected. In this work, noncoincidence detection of all the photofragments is employed to produce time-of-flight distributions that are used to investigate the D atom loss channel in DNCN photodissociation. The DNCN isotopomer was used rather than HNCN in order to optimize the detection of both fragments, as explained in Sec. II.

The experiments presented here show the D+NCN channel to be competitive with the previously observed CD $+\mathrm{N_2}$ channel. As this channel also appears to take place following internal conversion to the ground state, the results support NCN production from the HNCN intermediate formed in the $\mathrm{CH}+\mathrm{N_2}$ reaction.

II. EXPERIMENT

The fast beam photofragment translational spectrometer used in this study has been described in detail previously.[31–33] Briefly, a beam of internally cold radicals is produced by laser photodetachment of the corresponding mass-selected anions. The radicals then intersect a second laser pulse and undergo photodissociation, the fragments from which are detected on a photofragment imaging detector, yielding photofragment timing and position information used to characterize product translational energy and angular distributions.

$DNCN^-$ ions were produced from D_2NCN in a pulsed discharge source.[34] D_2NCN was synthesized by dissolving cyanamide (H_2NCN) in excess methanol-d_4 with ~1 vol. % acetic acid-d_4, stirring overnight, and evaporating the solvent under a stream of dry N_2. The source configuration used to produce $DNCN^-$ has been described previously.[2,35] Argon at a backing pressure of 2 atm was flowed through a pulsed valve into the region of the discharge plates. As D_2NCN has a very low vapor pressure at room temperature, it was placed in a reservoir between the pulsed valve and the discharge. The backing gas and the ions produced in the discharge underwent a supersonic expansion and were collimated by a skimmer. The ions were accelerated to a beam energy of 5 keV and focused by an Einzel lens. They were then separated by mass in a Bakker time-of-flight mass spectrometer.[36,37] The ion packet was intercepted by the output from a pulsed dye laser which detached an electron, and undetached ions were deflected from the beam path. The detachment laser energy in this study was tuned to 2.740 eV, slightly above the electron affinity of DNCN, 2.622 eV,[23] in order to produce internally cold radicals. The neutral radicals continued along the beam path to the photodissociation region, where they were intercepted by a second pulsed dye laser beam. The parent radicals and photofragments continued along the 2.15 m flight length to the detector.

The detector consists of 75 mm diameter microchannel plates mounted in a *Z*-stack configuration, coupled to a phosphor screen. A retractable $5 \times 8\ \mathrm{mm^2}$ beam block was positioned in the center of the detector to prevent the parent radicals from reaching the detector. Neutral fragments with laboratory kinetic energies exceeding 1 keV initiate an electron cascade upon striking the detector face, resulting in a spot on the phosphor screen. The image from the phosphor screen was split by a dichroic beam splitter, with the transmitted and reflected images focused onto an image intensifier in front of a charge-coupled device (CCD) camera and 4×4 multianode photomultiplier tube (PMT), respectively. Correlation of the CCD and PMT measurements yielded the position and arrival time, respectively, of each photofragment. Although the arrival times were of primary interest in the measurements reported here, the position information obtained from the CCD image was necessary for the determination of the exact location of the parent beam center and the beam block for each run.

The noncoincidence mode of operation used in this study[38] differed from the standard, coincidence mode[33] in that the fragment times and positions of impact were recorded regardless of whether the partner fragment or fragments from that dissociation event were detected. The timing data were converted into time-of-flight spectra, essentially measuring the distribution of fragment velocities along the ion beam axis. The resulting time-of-flight distribution was then fitted using a forward convolution fitting program, as described in Sec. III. Although no mass selection of the neutral fragments is performed, it will be seen that one can distinguish the contributions from the various photofragment

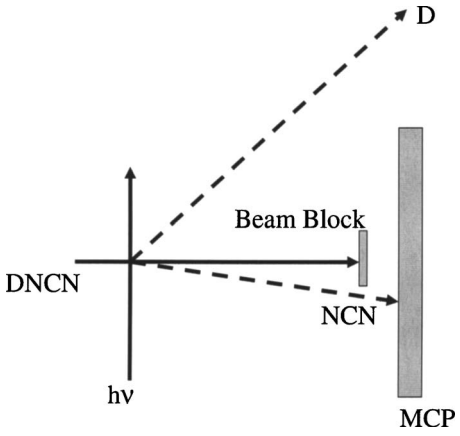

FIG. 2. Schematic showing the detector geometry for a noncoincident event. As can be seen, when enough energy is partitioned to the NCN fragment to bypass the beam block, the D cofragment recoils clear of the detector.

masses from the time-of-flight data and extract information on the translational energy and angular distribution for each detected channel, although this analysis is not as direct or precise as in the coincidence mode of detection.

The primary reason that noncoincidence detection was used in this study is that coincidence detection of the two fragments is possible only when the fragment mass ratio is less than about 10:1.[33] Otherwise, whenever the heavier fragment recoils with enough translational energy to clear the beam block and is thus detected, the lighter fragment either flies clear of the detector, as shown in Fig. 2, or is detected with low probability because of its small laboratory kinetic energy. Therefore, it is unlikely that both fragments from such a photodissociation event will be detected in coincidence, and channels such as reaction (5) cannot be studied. In contrast, noncoincidence detection allows the detection of product channels with a mass ratio greater than 10:1 as long as at least one of the fragments can be collected with reasonable efficiency. In this regard, the dissociation kinematics are still a consideration in the fragment detection efficiency. It is desirable that as many fragments as possible recoil with enough translational energy to clear the beam block, but not so much that they clear the detector. In order to optimize the chances of detecting at least one fragment, DNCN rather than HNCN was used in this study.

Excitation energies of 3.910, 4.035, and 4.158 eV were used in this study. These energies correspond to the maxima of vibronic transitions in the $\tilde{C}\,^2A'' \leftarrow \tilde{X}\,^2A''$ band and are the three lowest-energy transformations above the D–N bond dissociation energy that were previously found to lead to photodissociation, as well as the most intense transitions in the photofragment yield spectrum for this electronic band.[2] Both parallel and perpendicular dissociation laser polarizations relative to the beam axis were used in order to probe the photofragment angular distribution.

III. RESULTS AND ANALYSIS

A. Time-of-flight distributions

The time-of-flight distributions for DNCN photodissociation, with background subtraction, are shown as circles in Fig. 3. The background is higher at early times, resulting in higher base line noise after background subtraction. Data obtained with both parallel and perpendicular laser polarization are shown. The time-of-flight distributions are symmetric, reflecting the fact that the entire Newton sphere of recoiling photofragments is projected onto the detector. The signal at the center of the time-of-flight distributions corresponds to fragments with very little recoil velocity in the center-of-mass frame, while the events at the extreme ends correspond to those with significant recoil. Each spectrum comprises a narrow spike at the center of the distribution, with two shoulders on either side of the spike. Our past work showed CD $+N_2$ to be a major product channel from DNCN photodissociation. For each dissociation event, the recoil velocities of these fragments have a ratio of 2:1, so we expect the outer and inner shoulders to correspond to CD and N_2 fragments, respectively, a result supported by the analysis given below. The central spike should then be from NCN fragments, as these have very low recoil velocities owing to the high fragment mass ratio, 20:1, for the D+NCN channel. This assignment is supported by the observation that the central spike disappears at excitation energies below the D–NCN bond strength, 3.72 eV.

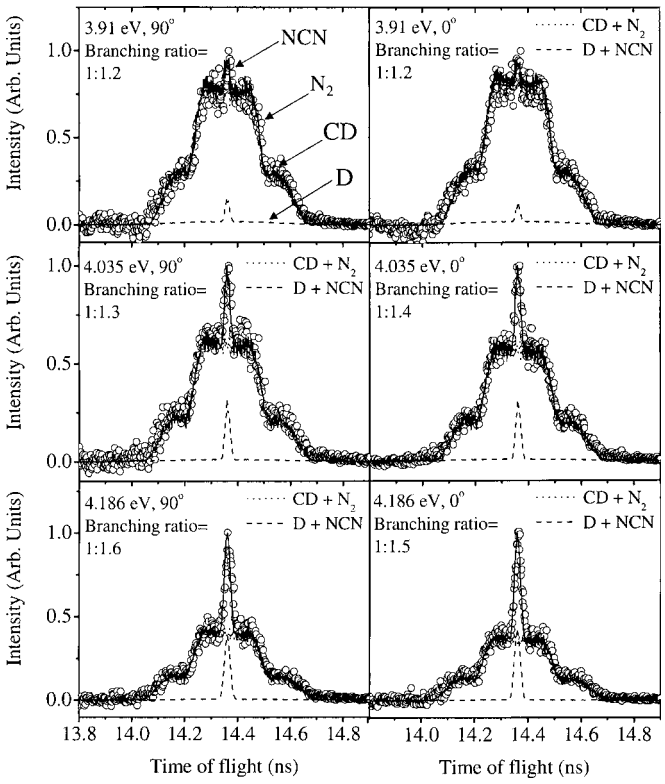

FIG. 3. Noncoincident time-of-flight spectra taken at photodissociation energies of 3.91, 4.035, and 4.186 eV with photodissociation light polarized both parallel and perpendicular to the beam axis. The open circles are experimental data and the lines are forward convolution fits to the data. The dotted lines correspond to fragments from the $CD+N_2$ channel, while the dashed lines correspond to fragments from the D+NCN channel. The sharp, central spike in the center of the spectra corresponds to the heavy NCN photofragment.

The fitting of these data, described in detail previously,[38,39] makes use of a forward convolution program to simulate the experimental time-of-flight distribution. A

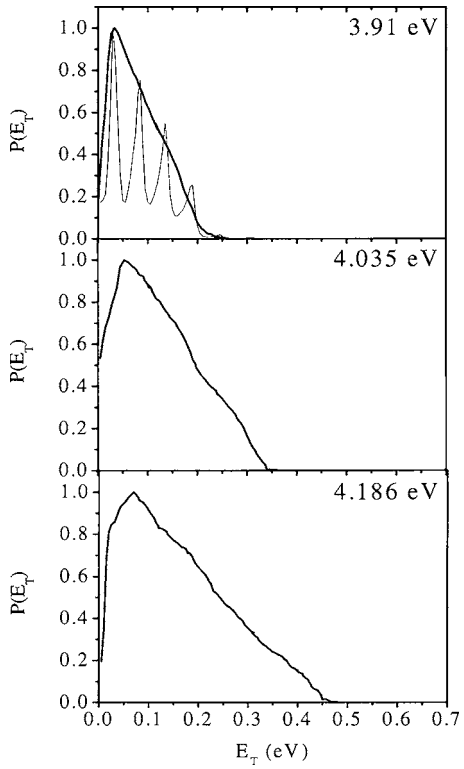

FIG. 4. Translational energy ($P(E_T)$) distributions derived from smoothing phase space theory (PST) calculations. The $P(E_T)$ distributions were then inserted into a forward convolution program to yield the spectra in Fig. 3. At 3.91 eV, the unsmoothed distribution used to generate the smoothed distribution is also shown.

translational energy distribution $P(E_T)$ and anisotropy parameter β are input for each product channel, and the time-of-flight distribution that would be observed in our experimental setup is simulated on the basis of the apparatus and detector geometry. The two dimensional fragment translational energy and angular distribution $P(E_T, \theta)$ is determined in the simulation from the equation[40]

$$P(E_T, \theta) = P(E_T)[1 + \beta P_2(\cos\theta)].$$

The $P(E_T)$ distribution and β parameter for the CD $+N_2$ channel are already known from our earlier study using coincidence detection, in which we found that $\beta=0$.[2] Using this information in our forward convolution program yielded the dotted lines in the time-of-flight plots in Fig. 3. The $CD+N_2$ contribution represents most of the time-of-flight signal and is therefore masked by the total contribution (solid line); it fits the two shoulders in the TOF spectra very well.

The remainder of the time-of-flight distributions, comprising primarily the sharp central feature, was fitted using the $P(E_T)$ distributions shown in Fig. 4 with isotropic angular distributions ($\beta=0$). A detection efficiency of the D atom relative to the NCN fragment of 8% was used,[41] although no discernible difference was seen upon increasing the efficiency to 20%.

The $P(E_T)$ distributions in Fig. 4 are smoothed distributions obtained from phase space theory (to be discussed in Sec. III B). A sample phase space theory distribution without smoothing is overlaid with the $P(E_T)$ used to fit the 3.91 eV time of flight in the top panel of Fig. 4. The error bars on β were found to be ±0.2, indicating that only a nearly isotropic angular distribution could be used to fit the data.

It is possible, in principle, to simulate the noncoincident photofragment position data using the same parameters as for the time-of-flight distributions, but we have not done this as there is little new information to be obtained. The noncoincident images show a cluster of points near the detector center corresponding to NCN fragments that have missed the beam block (which appears as a dark square at the center of the image, as seen previously[32]). The distribution of these events is isotropic, consistent with the near-zero anisotropy parameter obtained for this channel from simulating the time-of-flight data.

The contribution of the D+NCN channel and the total simulated time-of-flight spectra are shown in Fig. 3 as dashed and solid lines, respectively. The branching ratio ($CD+N_2$:D+NCN) is shown for each excitation energy. As mentioned in the Sec. II, a retractable beam block is used to prevent any undissociated parent radicals from striking the detector, leaving the center of the detector void of any dissociation products. Therefore, during data analysis, the center of the detector must be discriminated against so as to reproduce the experimental time of flight. Upon data analysis, however, it was found that changing the area of discrimination resulted in changes to the branching ratio necessary to fit the data. The resulting uncertainty in the branching ratio was ~25% at the lowest excitation energy (where the fragments are slowest), while in all others it was <10%. The absolute shape of the $P(E_T)$ distribution required to fit the data was not unique, but the same general qualitative shape was necessary for an adequate fit to the data. Hence, there is some uncertainty in both the $P(E_T)$ distributions and the branching ratio, owing to low sensitivity to events with small translational energy release. While the intensity at very low translational energy (~0–0.075 eV) cannot be determined with great certainty, it is clear that the $P(E_T)$ distributions peak close to $E_T=0$.

Although the branching ratio appears to increase in favor of the D+NCN channel with increasing photon energy, this increase is within the experimental uncertainty of the branching ratio. The observed increase in the intensity of the sharp central peak with photon energy is due not only to the possible increase in branching ratio but also to an increased number of heavy NCN fragments with enough translational energy to clear the beam block successfully and be detected.

B. Phase space theory calculations

Phase space theory[42] calculations were performed in order to determine whether the $P(E_T)$ distributions found for the D+NCN channel can be fitted with this simple statistical model. Our procedure for performing phase space theory calculations has been described in detail previously.[43] The vibrational density of states is calculated using the Beyer-Swinehart algorithm, and we determine the centrifugal barrier assuming a long-range potential of the form $V(r) = -C_0/r^6$. The molecular constants for DNCN used as input

for the phase space theory calculations were determined from electronic structure calculations using the B3LYP method with the 6-311++G(2*df*,*p*) basis set, carried out using the GAUSSIAN03 program package.[44]

IV. DISCUSSION

In this section, we consider what can be learned about the dissociation mechanism from the observed product distributions. The first point is to determine whether dissociation to D+NCN occurs on an excited electronic state or on the ground state. The narrow bands in the spectrum of the $\tilde{C}\,^2A'' \leftarrow \tilde{X}\,^2A''$ transition rule out direct dissociation from the $\tilde{C}\,^2A''$ state.[2] The observed isotropic distribution ($\beta=0$) also suggests that the dissociation does not take place directly. Either direct dissociation or dissociation over a barrier is also precluded by the fact that the translational energy distributions peak very close to $E_T=0$. Since the observed $P(E_T)$ distributions used to fit the time-of-flight spectra were modified from those derived from phase space theory, they indicate statistical dissociation without a reverse barrier, as would be the case if dissociation occurred following internal conversion to the ground state. It appears, therefore, that internal conversion to the ground electronic state occurs prior to dissociation and that the nature of the reaction coordinate is as predicted by Moskaleva *et al.*,[1] i.e., no exit barrier with respect to the products.

In our previous study of dissociation following excitation of the $\tilde{C}\,^2A'' \leftarrow \tilde{X}\,^2A''$ transition,[2] the $P(E_T)$ distributions for the $CH+N_2$ were also explained in terms of internal conversion to the ground state. These distributions were structured and peaked well away from $E_T=0$ and were attributed to isomerization to cyclic HCN_2 followed by passage over a tight transition state *en route* to dissociation, TS3 in Fig. 1. Hence, both channels seen in the current study appear to result from internal conversion to the ground state. The approximately equal branching to $CD+N_2$ and D+NCN observed here can then be rationalized in terms of the competition between dissociation over a lower-energy but tight transition state, TS3, predicted to lie 3.217 eV above HNCN, and the higher-lying, loose transition state associated with dissociation to D+NCN. The key point, however, is that our results indicate a facile path to the formation of the HNCN intermediate from $CH+N_2$ reactants, and once HNCN is formed, it can dissociate relatively efficiently to H+NCN products. Hence, our results provide experimental support for the mechanism for prompt NO formation proposed by Moskaleva *et al.*

V. CONCLUSIONS

This study shows that D+NCN products are formed from excitation of DNCN in the range of a few hundred meV above the bond dissociation energy. The translational energy distributions for this channel are consistent with statistical dissociation on the ground state surface, making the results relevant to reactions proposed to be important in prompt NO formation. The branching ratios ($D+NCN:CD+N_2$) are close to 1:1. Overall, our results are consistent with the potential energy surface determined by Moskaleva *et al.*[1] for the reaction pathway from $CH+N_2$, through the HNCN intermediate, to H+NCN.

ACKNOWLEDGMENT

This work was supported by the Director, Office of Basic Energy Sciences, Chemical Sciences Division of the U. S. Department of Energy under Contract No. DE-AC02-05CH11231.

[1] L. V. Moskaleva, W. S. Xia, and M. C. Lin, Chem. Phys. Lett. **331**, 269 (2000).
[2] R. T. Bise, A. A. Hoops, and D. M. Neumark, J. Chem. Phys. **114**, 9000 (2001).
[3] C. P. Fenimore, *Proceedings of the 13th Symposium (International) on Combustion* (The Combustion Institute, Pittsburgh, 1971), p. 373.
[4] J. A. Miller and C. T. Bowman, Prog. Energy Combust. Sci. **15**, 287 (1989).
[5] J. Blauwens, B. Smets, and J. Peeters, *Proceedings of the 16th Symposium (International) on Combustion* (The Combustion Institute, Pittsburgh, 1977), p. 1055.
[6] M. R. Berman and M. C. Lin, J. Phys. Chem. **87**, 3933 (1983).
[7] A. J. Dean, R. K. Hanson, and C. T. Bowman, *Proceedings of the 23rd Symposium (International) on Combustion* (The Combustion Institute, Pittsburgh, 1990), p. 259.
[8] D. Lindackers, M. Burmeister, and P. Roth, *Proceedings of the 23rd Symposium (International) on Combustion* (The Combustion Institute, Pittsburgh, 1990), p. 251.
[9] M. R. Manaa and D. R. Yarkony, Chem. Phys. Lett. **188**, 352 (1992).
[10] L. J. Medhurst, N. L. Garland, and H. H. Nelson, J. Phys. Chem. **97**, 12275 (1993).
[11] J. M. L. Martin and P. R. Taylor, Chem. Phys. Lett. **209**, 143 (1993).
[12] T. Seidman, J. Chem. Phys. **101**, 3662 (1994).
[13] D. Fulle and H. Hippler, J. Chem. Phys. **105**, 5423 (1996).
[14] A. S. Rogers and G. P. Smith, Chem. Phys. Lett. **253**, 313 (1996).
[15] J. A. Miller and S. P. Walch, Int. J. Chem. Kinet. **29**, 253 (1997).
[16] S. D. Le Picard, A. Canosa, B. R. Rowe, R. A. Brownsword, and I. W. M. Smith, J. Chem. Soc., Faraday Trans. **94**, 2889 (1998).
[17] Q. Cui, K. Morokuma, J. M. Bowman, and S. J. Klippenstein, J. Chem. Phys. **110**, 9469 (1999).
[18] A. Wada and T. Takayanagi, Chem. Phys. **116**, 7065 (2002).
[19] A. E. Faulhaber, J. R. Gascooke, A. A. Hoops, and D. M. Neumark, J. Chem. Phys. **124**, 204303 (2006).
[20] G. P. Smith, Chem. Phys. Lett. **367**, 541 (2003).
[21] M. Wu, G. Hall, and T. J. Sears, J. Chem. Soc., Faraday Trans. **89**, 615 (1993).
[22] S. Yamamoto and S. Saito, J. Chem. Phys. **101**, 10350 (1994).
[23] E. P. Clifford, P. G. Wenthold, W. C. Lineberger, G. A. Petersson, and G. B. Ellison, J. Phys. Chem. A **101**, 4338 (1997).
[24] H. W. Kroto, T. F. Morgan, and H. H. Sheena, Trans. Faraday Soc. **66**, 2237 (1970).
[25] G. Herzberg and P. A. Warsop, Can. J. Phys. **41**, 286 (1963).
[26] G. Herzberg and D. N. Travis, Can. J. Phys. **42**, 1658 (1964).
[27] N. Basco and K. K. Yee, Chem. Commun. (London) **3**, 150 (1968).
[28] T. Takayanagi, Chem. Phys. Lett. **368**, 393 (2003).
[29] F.-M. Tao, M. C. McCarthy, C. A. Gottlieb, and P. Thaddeus, J. Chem. Phys. **100**, 3691 (1994).
[30] C. Puzzarini and A. Gambi, J. Chem. Phys. **122**, 064316 (2005).
[31] R. E. Continetti, D. R. Cyr, R. B. Metz, and D. M. Neumark, Chem. Phys. Lett. **182**, 406 (1991).
[32] A. A. Hoops, J. R. Gascooke, A. E. Faulhaber, K. E. Kautzman, and D. M. Neumark, Chem. Phys. Lett. **374**, 235 (2003).
[33] A. A. Hoops, J. R. Gascooke, K. E. Kautzman, A. E. Faulhaber, and D. M. Neumark, J. Chem. Phys. **120**, 8494 (2004).
[34] D. L. Osborn, D. J. Leahy, D. R. Cyr, and D. M. Neumark, J. Chem. Phys. **104**, 5026 (1996).
[35] T. R. Taylor, R. T. Bise, K. R. Asmis, and D. M. Neumark, Chem. Phys. Lett. **301**, 413 (1999).
[36] J. M B. Bakker, J. Phys. E **7**, 364 (1974).
[37] J. M. B. Bakker, J. Phys. E **6**, 785 (1973).

[38] A. E. Faulhaber, D. E. Szpunar, K. E. Kautzman, and D. M. Neumark, J. Phys. Chem. A **109**, 10239 (2005).
[39] D. R. Cyr, R. E. Continetti, R. B. Metz, D. L. Osborn, and D. M. Neumark, J. Chem. Phys. **97**, 4937 (1992).
[40] R. N. Zare, Mol. Photochem. **4**, 1 (1972).
[41] D. L. Osborn, D. J. Leahy, and D. M. Neumark, J. Phys. Chem. A **101**, 6583 (1997).
[42] P. Pechukas and J. C. Light, J. Chem. Phys. **42**, 3281 (1965).
[43] H. Choi, R. T. Bise, A. A. Hoops, D. H. Mordaunt, and D. M. Neumark, J. Phys. Chem. A **104**, 2025 (2000).
[44] M. J. Frisch, G. W. Trucks, H. B. Schlegel *et al.*, GAUSSIAN03, Revision C.02, Gaussian, Inc., Pittsburgh, PA, 2003.